ACS APPLIED MATERIALS & INTERFACES

Research Article

www.acsami.org

Exploring Graphene Nanocolloids as Potential Substrates for the Enhancement of Raman Scattering

Shengtong Sun, Zehui Zhang, and Peiyi Wu*

State Key Laboratory of Molecular Engineering of Polymers, Ministry of Education, Department of Macromolecular Science, and Laboratory of Advanced Materials, Fudan University, Shanghai 200433, People's Republic of China

Supporting Information

ABSTRACT: Graphene, especially few-layer graphene solid film, has been found to strongly suppress fluorescence and enhance Raman signals of probe molecules. In this paper, we attempt to explore the possibility of using graphene nanocolloids as potential substrates for the enhancement of Raman scattering. Graphene nanocolloids chemically produced from the reduction of graphene oxide by sodium citrate are nearly all monolayers in solution and are also found to exhibit certain surface-enhanced Raman scattering (SERS) activity to common aromatic probe molecules. Interestingly, largely different from few-layer graphene solid film, graphene nanocolloids show maximal SERS activity only when the probe molecules are at resonant laser excitation. According to our analysis, this phenomenon should arise from a combined effect of fluorescence quenching of graphene and a photoinduced charge transfer mechanism, in which the strong charge transfer accounts for the main contribution from close coupling between graphenes and probe molecules photoinduced by resonant excitation as well as the desolvation of graphene sheets and probe molecules.

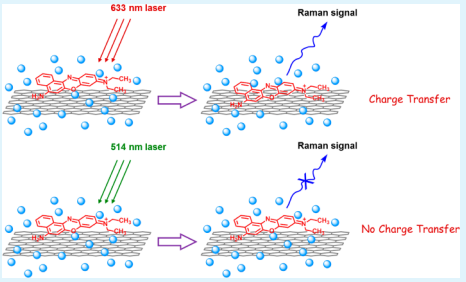

KEYWORDS: *graphene nanocolloids, surface-enhanced Raman scattering, probe molecules, photoinduced charge transfer, resonant excitation, desolvation, surface coupling*

1. INTRODUCTION

Since its inception in the late 1970s, surface-enhanced Raman scattering (SERS), as an ultrasensitive method for the detection of analytes even at the single-molecule level, has stimulated great interest, even in recent years.[1,2] Despite numerous theoretical and experimental works, the origins of the SERS effect are still in dispute, which are attributed to three possible sources: electromagnetic enhancement based on surface plasmon resonance (10^6–10^8-fold enhancement), chemical enhancement based on charge transfer (usually 10–100-fold enhancement), and resonances within the molecule itself.[3,4] To distinguish and quantitate these three effects is rather difficult, especially in traditional metal-substrated systems, because they often occur simultaneously.[5,6]

Recently, graphene was found to strongly suppress fluorescence and enhance Raman signals of probe molecules.[7] Because of its relatively smooth surface, strong optical transmission (>95%), and surface plasmon range in terahertz, SERS of graphene, also named graphene-enhanced Raman spectroscopy (GERS), was attributed to a chemical enhancement mechanism.[8] Several characteristics of the charge transfer such as the "first-layer effect"[9] and a Fermi-level dependence of GERS with a changing electrical field[10,11] also support this conclusion. Additionally, new reports stated that the chemical enhancement of graphene can be modulated by changing the chemical reduction of graphene oxide sheets[12] or by UV–ozone treatment[13] because of the incorporation of electronegative oxygen species. Thus, graphene is regarded as an ideal substrate for studying the chemical enhancement mechanism exclusively. However, a recent study by Thrall et al. found that as for rhodamine 6G (R6G) adsorbed on bilayer graphene at resonant excitation, the Raman scattering cross section is actually reduced from its solution value, and mainly optical strong quenching of fluorescence makes for sensitive Raman detection.[14] The detailed mechanism of graphene-based Raman enhancement may need to be clarified further.

Moreover, nearly all previous reports of GERS were based on the deposition of molecules on graphene sheets. Although strong Raman enhancement may be realized by this method, the reproductivity and uniformity of Raman signals are limited by the random sizes and distribution of graphene sheets as well as dye aggregation. On the other hand, the enhanced efficiency is also closely related to the number of layers of graphene, with a drastic decrease in the SERS effect from monolayers to multilayers (called "*n*-layer effect").[15] Besides, it is usually time-consuming to fabricate graphene devices and to identify graphene sheets with different layers by optical microscopy. As water is a weak Raman scatterer, noble metal (mostly Au and Ag) nanocolloids are also commonly used as SERS substrates, especially in biomedical applications with good reproductivity and operability.[16,17] However, noble metal nanocolloids are usually environmentally unstable, which may

Received: March 14, 2013
Accepted: May 2, 2013
Published: May 2, 2013

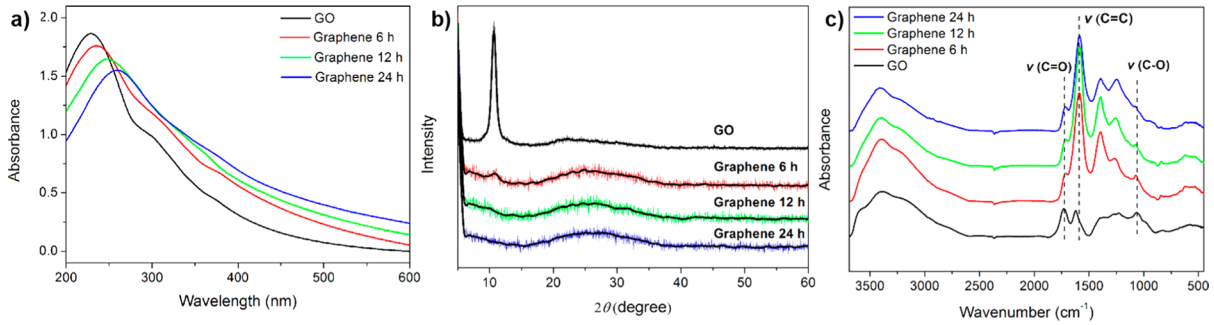

Figure 1. (a) UV−vis spectra of GO and RGO aqueous dispersions as a function of reduction time (6, 12, or 24 h). (b) XRD and (c) FTIR characterization of dried GO and RGO as a function of reduction time.

cause the loss of SERS activity by oxidation, agglomeration, or fragmentation.[18,19] A graphene nanocolloid is an alternative method of overcoming this problem because of its high surface activity, biocompatibility, and environmental stability.[20] Therefore, in this paper, we attempt to investigate the SERS activity of graphene nanocolloids, which are environmentally obtained by reducing graphene oxide (GO) with sodium citrate. We find that graphene nanocolloids can also be used as potential substrates for the enhancement of Raman scattering, and a distinct absorption wavelength-dependent phenomenon is also discovered, which should arise from a combined effect of fluorescence quenching of graphene and a photoinduced charge transfer mechanism. Herein, graphene sheets are nearly all monolayers in solution where the *n*-layer effect can be easily avoided.

2. EXPERIMENTAL SECTION

2.1. Preparation of GO. GO was successfully prepared by a modified Hummers' method.[21] Briefly, expandable graphite powders (5 g, 8000 mesh, Aladdin Co. Ltd.) and sodium nitrate (2.5 g) were mixed in concentrated H_2SO_4 (115 mL) at 0 °C, followed by the addition of potassium permanganate (15 g) under vigorous stirring. After the temperature had been increased to 35 °C, excess deionized water (300 mL) was added to the mixture before it was stirred for 30 min. The temperature was then increased to 90 °C before the addition of 30% H_2O_2 (100 mL). The resulting suspension was filtered, washed with 5% HCl, and dialyzed for 7 days to remove the remaining metal species. The GO aqueous dispersion was diluted before being used.

2.2. Reduction of GO by Sodium Citrate. A mixed aqueous solution of GO (0.3 mg/mL) and sodium citrate [10 mg/mL (Sigma-Aldrich)] was maintained at 100 °C for a specified period of time (6, 12, or 24 h). After the mixture had cooled to room temperature, the supernatant solution was discarded and the reduced GO (RGO) platelets in water were redispersed by ultrasonication for 0.5 h. The resultant RGO aqueous dispersion was dialyzed for 5 days and diluted to 0.1 mg/mL before being used.

2.3. Characterization. Atomic force microscopic (AFM) images were obtained using a Multimode Nano 4 instrument in tapping mode. For AFM observations, the RGO dispersion was diluted (0.2 mg/mL) and then spin-coated onto freshly cleaved mica surfaces. Transmission electron microscope (TEM) images were taken with a JEOL JEM 2011 instrument at 200 kV equipped with electron diffraction (ED). The analysis of X-ray photoelectron energy spectra (XPS) was performed using an RBD upgraded PHI-5000CESCA system (Perkin-Elmer) with Mg Kα radiation ($h\nu$ = 1253.6 eV). X-ray diffraction (XRD) patterns were acquired by a D8 ADVANCE and DAVINCI.DESIGN (Bruker) X'pert diffractometer with Cu Kα radiation. Thermogravimetric analysis (TGA) was performed under a nitrogen atmosphere with a Perkin-Elmer thermal analyzer at a heating rate of 20 °C/min. Fourier transform infrared (FTIR) spectra were recorded on a Nicolet Nexus 470 spectrometer. Ultraviolet−visible (UV−vis) spectra of all dye molecules (purchased from Aladdin Co. Ltd.) in aqueous solutions were measured on a Hitachi U-2910 spectrophotometer. Fluorescence emission spectra and the fluorescence delay of R6G and RhB with and without graphene in aqueous solutions were measured on an Edinburgh Ins FLS920 spectrophotometer. The mixed aqueous solutions of the graphene nanocolloid (0.1 mg/mL) and probe molecule were sealed in capillary tubes for Raman measurement. Raman and SERS spectra were recorded on a Renishaw inVia Reflex micro-Raman spectrometer with He/Ne laser excitation at 633 and 514 nm. A 200× objective was used to focus the laser beam and to collect the Raman signal. To ensure the obtained spectra were comparable, the settings, including the laser power and exposure time, were all the same.

3. RESULTS AND DISCUSSION

3.1. Characterization of Graphene Nanocolloids. To obtain good water dispersibility, graphene nanocolloids were prepared by reducing GO with sodium citrate directly in water.[22] The success of the reduction of GO can be clearly evidenced by the obvious change in color from light brown to black (Figure S1a of the Supporting Information). By being washed and dialyzed, RGO can be well redispersed in water without the assistance of any stabilizing agents. AFM and TEM images of RGO sheets (Figure S1b,c of the Supporting Information) show that RGO sheets have an average thickness of 0.75 nm, indicating the stable existence of single-layer graphene sheets in water, and RGO sheets are well-crystallized with a regular carbon framework determined from the ED pattern.[23] On the other hand, the reduction process can be monitored by time-dependent UV−vis spectra, as shown in Figure 1a. As the reduction reaction proceeds, the UV−vis absorption peak of GO at 229 nm gradually red shifts to 260 nm corresponding to the restored conjugated structure within graphene sheets.[24] From XRD patterns in Figure 1b, we can observe the apparent disappearance of the characteristic diffraction peak of GO at 10.7° with an ~0.82 nm interlayer spacing as GO was reduced. Determined from FTIR spectra in Figure 1c, three peaks can be identified: C═O stretching band at 1724 cm^{-1}, C═C stretching band at 1587 cm^{-1}, and C−O stretching band at 1065 cm^{-1}. Obviously, as GO was reduced, C−O groups gradually disappeared while C═C groups from the graphitic basal planes emerged. Other characterizations such as Raman, TGA, and XPS (Figures S2−S4 of the Supporting Information) also support the successful reduction of GO and the increasing reduction degree that is dependent on the reduction time.

3.2. Raman Enhancement of Graphene Nanocolloids. Unless otherwise stated, the concentrations of graphene in all the solutions used for Raman measurement were fixed to 0.1 mg/mL. We have previously reported that noble metal

nanoparticle-decorated graphene sheets as well as graphene sheets individually both have a Raman signal enhancement of nile blue A (NBA) at 10^{-4} M,[25] in which the interfering excited state luminescence of NBA was effectively quenched. Thus, graphene nanocolloids can be used as potential SERS substrates. It should be noted that a competitive effect also exists in the SERS of graphene nanocolloids. That is, because of the strong solvation of graphene sheets and probe molecules in water, the Raman enhancement is relatively weak. As the concentration of probe molecules is $<10^{-5}$ M, the Raman signal of probes enhanced by graphene would be overlapped by that of graphene itself and thus is difficult to identify (Figure S5 of the Supporting Information), to which researchers need to pay careful attention; 10^{-4} M is most suitable and thus was chosen for investigating SERS of graphene nanocolloids in this paper.

We first examined the dependence of SERS of NBA at its resonant excitation in graphene nanocolloids on the reduction time, as shown in Figure 2. No Raman signal can be detected in

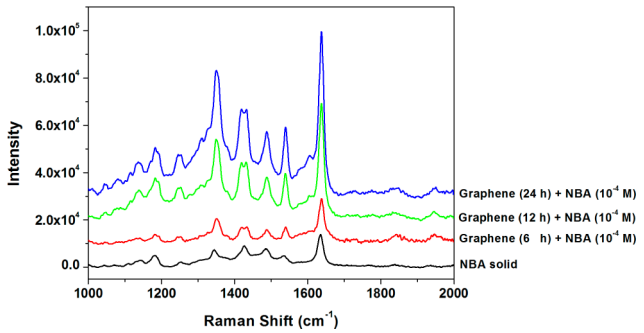

Figure 2. Background-subtracted Raman spectra of NBA (10^{-4} M) in graphene aqueous solutions (0.1 mg/mL) with different reduction times at 633 nm laser excitation.

GO nanocolloids except for a strong fluorescence peak. As the reduction time is extended, the Raman signal of NBA is gradually enhanced. It is supposed that with the increase in the reduction time, more conjugated structures are restored, which is necessary for the origins of Raman enhancement by charge transfer and fluorescence quenching between graphene surfaces and probe molecules. We measured the surface density of NBA molecules on GO and RGO by UV–vis absorption spectra at 636 nm (as shown in Figure S6 of the Supporting Information). The surface densities of NBA molecules on GO and RGO (6, 12, or 24 h) (depicted by $n_{NBA}/m_{graphene}$) are roughly calculated to be 0.78, 0.63, 0.73, and 0.77 mol/mg, corresponding to adsorption ratios of 78, 63, 73, and 77%, respectively (10^{-4} M NBA without graphene as a reference). Note that the high surface density of NBA on GO should be caused by both strong electrostatic attraction (NBA molecules are positively charged) and $\pi-\pi$ stacking. The dependence of surface adsorption density on the reduction time of graphene supports the idea that the Raman enhancement of graphene nanocolloids most likely arises from charge transfer and/or fluorescence quenching between conjugated graphene surfaces and probe molecules.

It is also noted that this regularity is inconsistent with the direct deposition of molecules on graphene sheets where the maximal Raman enhancement occurs on mildly reduced RGO nanosheets.[12] The probable reason may be that in aqueous solutions the electrostatic adhesion is strongly weakened by the solvation effect. Thus, in solutions, $\pi-\pi$ stacking coupling is the key to the degree of Raman enhancement. Another phenomenon that should be noted is that even if there is very weak fluorescence emission for NBA, with a reduction time of 24 h, the fluorescence background is still 4–6 times greater than the Raman signal (not shown). It reveals that a graphene nanocolloid has relatively weaker fluorescence suppressing ability than a graphene solid film because of the solvation effect. This is important for us to distinguish the contributions to Raman enhancement from charge transfer and/or resonance of dyes enhanced by fluorescence quenching.

We are also very interested in the SERS effect of graphene nanocolloids on different probe molecules with different conjugated structures and absorption wavelengths. Table 1

Table 1. Abbreviations and Absorption Peaks of Dye Molecules Used as SERS Probes[a]

name	abbreviation	absorption peak (nm)
crocein orange	COG	484
natural red	NR	535
rhodamine 6G	R6G	527
rhodamine B	RhB	557
crystal violet	CV	585
brilliant blue R	BB	555
methyl blue	MB	585
nile blue A	NBA	636
toluidine blue	TB	628
azure I	–	660
methylene blue	MEB	665

[a]See Figures S7 and S8 of the Supporting Information for corresponding structures and absorption profiles.

lists all the dye molecules we used as SERS probes as well as their absorption peaks, which show a gradual color shift from red to blue. Surprisingly, graphene nanocolloids selectively enhance the Raman signals of probe molecules in a manner that is strongly dependent on the laser excitation wavelength, as shown in Figure 3. That is, under 633 nm laser excitation, only the Raman signals of blue and violet dye molecules can be enhanced, while the Raman signals of red and orange dye molecules are heavily overlapped by that of graphene. Under 514 nm laser excitation, the order is just the opposite. Note that no Raman signals can be detected for R6G and RhB under 514 nm laser excitation because of overly strong fluorescence emission.

It is interesting to examine the relationship between the absorption wavelength of dye molecules and the laser excitation wavelength. They are closely matched. In other words, the dye molecules have the maximal Raman enhancement by graphene nanocolloids at their resonant excitation. As we know, for Au or Ag nanocolloids as SERS substrates obeying an electromagnetic enhancement mechanism, to select a laser with its excitation away from the absorption wavelength to avoid the inferring fluorescence is essential for a successful Raman signal detection. However, it is not always effective for specified systems, e.g., the interference from other impurity species with strong fluorescence. Graphene nanocolloids can be an alternative SERS substrate for filling the gaps.

Essentially, the origin of SERS by graphenes is from the competitive result of fluorescence of probe molecules and the Raman signal enhanced by charge transfer interaction. In the case of a metallic surface, this effect is closely related to the distance between probe molecules and surfaces. As the probe

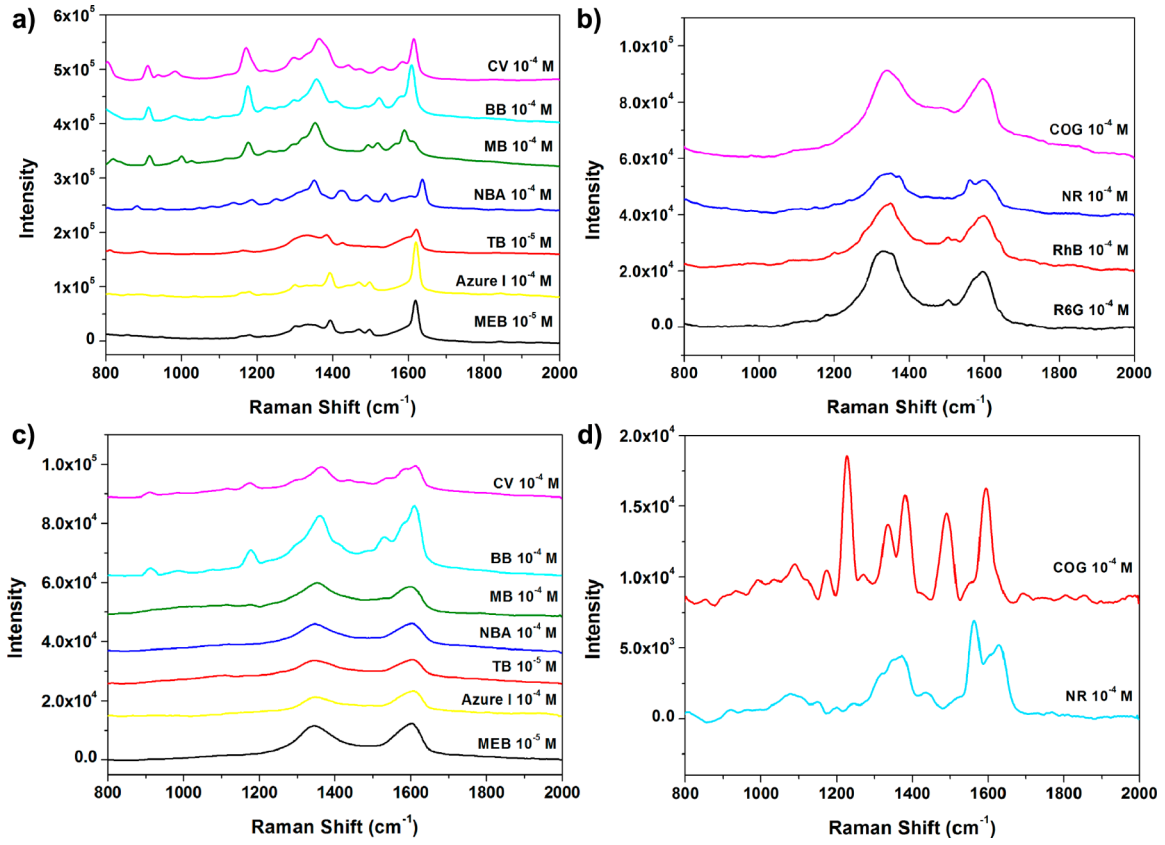

Figure 3. Background-subtracted Raman spectra of different probe molecules (10^{-4} M) in graphene aqueous solutions (0.1 mg/mL) at 633 nm laser excitation (a and b) and 514 nm laser excitation (c and d).

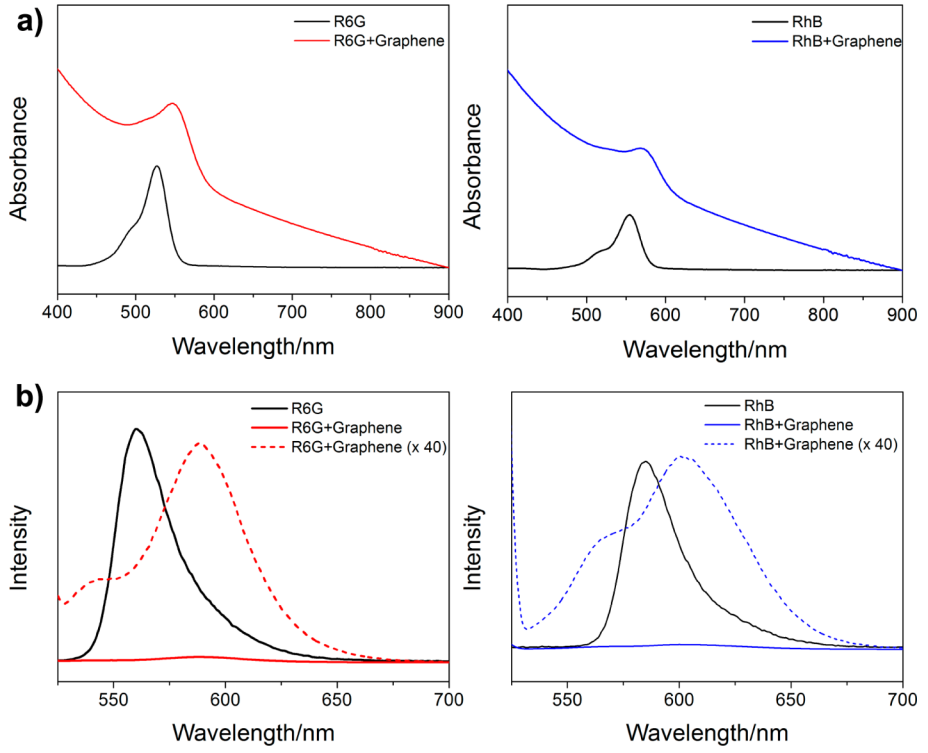

Figure 4. (a) UV−vis absorption spectra of R6G and RhB with and without graphenes. (b) Fluorescence emission spectra of R6G and RhB (10^{-4} M) at 514 nm excitation with and without graphenes (0.1 mg/mL). The dotted lines represent 40-fold enlarged spectra of graphene/dye solutions.

molecules move closer to the surface, fluorescence is further quenched while SERS emerges.[16] However, in graphene nanocolloids, distinguishing the coexisting Raman signals enhanced by fluorescence quenching and those by charge

transfer at resonant excitation is very difficult. This is because these two contributions are all based on the coupling between graphene surfaces and probe molecules.

To discern these two contributions, we first examined the detailed enhanced Raman signals in Figure 3. A closely matched relationship between the absorption wavelength of blue and red dyes and the laser excitation wavelength can be obviously observed as mentioned above. However, it is also noted that the Raman signal of crystal violet (CV) at 633 nm excitation (where its absorption is very weak, as shown in Figure S8 of the Supporting Information) is as strong as that of blue dyes at their resonant excitation (Figure 3a). Similarly, crocein orange (COG) at 514 nm nonresonant excitation also exhibits enhanced Raman signals (Figure 3d). At 633 nm nonresonant excitation, red and orange dyes still show small but recognizable Raman signals (Figure 3b). These observations reveal that the chemical enhancement by charge transfer may account for the main contribution to the SERS activity of graphene nanocolloids.

Second, as we stated above, no Raman signals can be detected for R6G and RhB under 514 nm laser excitation because of strong fluorescence emission. On the other hand, on few-layer graphenes prepared either by soaking in the solution or by vacuum evaporation, R6G even at very low concentration shows clear Raman signals at resonant excitation by fluorescence quenching.[7,8,14] It indicates that graphene nanocolloids have relatively weaker fluorescence suppressing ability than a graphene solid film because of the solvation effect.

To examine the coupling between graphene surfaces and dye molecules, we plotted the UV−vis absorption spectra and fluorescence emission spectra of R6G and RhB as shown in Figure 4. With the addition of graphenes, the absorption peaks of R6G and RhB are broadened and red shift to 548 and 572 nm, respectively, suggesting in the ground state the close attachment of dye molecules on graphene surfaces by $\pi-\pi$ coupling interactions. Similar phenomena can also be observed in other graphene/dye hybrid systems.[26−28] Because the absorption in graphene/dye solutions for free dyes is very low (Figure 4a, not considering the background from graphenes), most dye molecules are coupled on graphene surfaces, in accordance with our former surface density analysis of NBA molecules on graphene sheets. This can also be supported by fluorescence emission spectra. Graphene shows nearly 40-fold fluorescence quenching toward R6G and RhB, quite higher than the levels reported previously with a 1:1 graphene:RhB weight ratio.[28] Such high fluorescence quenching efficiency could be due to an electron (charge) or energy transfer pathway of excited state deactivation. As reported, π-interactions between aromatic molecules and graphenes are supposed to produce significant charge transfer effects.[29]

Additionally, fluorescence decay measurements also supported the existence of photoinduced electron or energy transfer phenomena.[29,30] As shown in Figure S9 of the Supporting Information, at 514 nm excitation, R6G and RhB show monoexponential delays with lifetimes of 4.75 and 2.13 ns, respectively. Addition of graphene causes the lifetimes to decrease to 4.33 and 2.01 ns, respectively. Distinguishing the electron or energy transfer processes may require further fluorescence analysis on a faster time scale such as laser flash photolysis to explore the transient species.[30] Nevertheless, considering an even much higher quenching efficiency in a graphene solid film (~10^3 times as reported previously[7]), we ascribed the enhancement of Raman scattering in graphene nanocolloids mainly to chemical enhancement by a photoinduced charge transfer phenomenon.

In graphene nanocolloids, the graphene nanosheets and probe molecules are all solvated, which subsequently leads to the loose coupling between graphene surfaces and probe molecules. The loose coupling is not favorable for the occurrence of charge transfer that needs close contact between probes and substrates. Interestingly, except for an obvious red-shifted emission peak in the fluorescence spectra of graphene/dye solutions (Figure 4b), we observe a shoulder peak with a wavelength lower than that of dye molecules without graphene. This peak can be attributed to the formation of dye aggregates induced by desolvation.[14] Two reasons could account for this phenomenon. First, graphene is known to be sensitive to light stimuli, especially near-infrared light.[31,32] Under strong laser excitation, graphene would absorb light energy to induce the local temperature increase and the desolvation of graphene sheets and dye molecules. Second, as we stated in the fluorescence quenching analysis, under resonant excitation, a coherent photoinduced electron transfer occurs, which has also been proven by plenty of researchers.[33−36] In the excited state, probe molecules are subjected to the breathing of the hydration shell and an ultrafast intramolecular rearrangement that leads to the detachment of solvated clusters and a fluorescent charge transfer state of probes. These two processes are both very favorable to the close coupling between graphene surfaces and probe molecules, which subsequently induces the strong enhancement of Raman signals. With NBA as an example, the schematic mechanism is plotted in Figure 5. Resonant excitation (633 nm) causes the close contact between graphene and NBA molecules, resulting in a strong charge transfer and Raman signal enhancement.

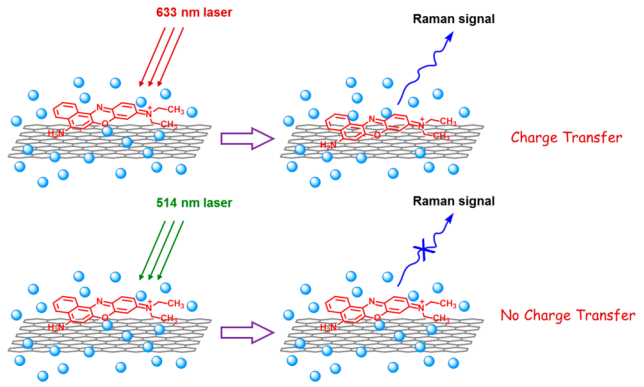

Figure 5. Schematic representation of Raman signal enhancement of NBA under resonant (633 nm) and nonresonant (514 nm) excitation.

4. CONCLUSION

In this paper, we attempt to explore the use of graphene nanocolloids as potential SERS substrates, which are found to show certain SERS activity on various probe molecules. Compared with noble metal nanocolloids and few-layer graphene solid film, graphene nanocolloids exhibit maximal Raman enhancement only when the probe molecules are at their resonant laser excitation. This phenomenon should result from a combination of the effect of fluorescence quenching of graphene and a photoinduced charge transfer mechanism. Meanwhile, the main contribution is from the strong charge transfer by close coupling between graphene surfaces and probe

molecules photoinduced by resonant excitation as well as the desolvation of graphene sheets and dye molecules, although its microscopic mechanism may need to be clarified further. The use of graphene nanocolloids as SERS substrates would make up for the deficiency of noble metal nanocolloids in selecting excitation lasers, which may be used in biomedical applications.

■ ASSOCIATED CONTENT

Ⓢ Supporting Information

AFM, TEM, Raman, TGA, and XPS characterization of GO and RGO; concentration-dependent Raman spectra of NBA, CV, and R6G; surface density analysis of NBA on GO and RGO; chemical structures and absorption profiles of all probe molecules; and fluorescence decay measurements of R6G and RhB with and without graphene. This material is available free of charge via the Internet at http://pubs.acs.org.

■ AUTHOR INFORMATION

Corresponding Author

*E-mail: peiyiwu@fudan.edu.cn.

Notes

The authors declare no competing financial interest.

■ ACKNOWLEDGMENTS

We gratefully acknowledge the financial support from the National Science Foundation of China (NSFC) (20934002 and 51073043) and the National Basic Research Program of China (2009CB930000).

■ REFERENCES

(1) Haran, G. *Acc. Chem. Res.* **2010**, *43*, 1135−1143.
(2) Tian, Z. Q.; Ren, B.; Wu, D. Y. *J. Phys. Chem. B* **2002**, *106*, 9463−9483.
(3) Lombardi, J. R.; Birke, R. L. *Acc. Chem. Res.* **2009**, *42*, 734−742.
(4) Qian, X. M.; Nie, S. *Chem. Soc. Rev.* **2008**, *37*, 912−920.
(5) Sanchez-Cortes, S.; Garcia-Ramos, J. *Langmuir* **2000**, *16*, 764−770.
(6) Park, W. H.; Kim, Z. H. *Nano Lett.* **2010**, *10*, 4040−4048.
(7) Xie, L.; Ling, X.; Fang, Y.; Zhang, J.; Liu, Z. *J. Am. Chem. Soc.* **2009**, *131*, 9890−9891.
(8) Ling, X.; Xie, L.; Fang, Y.; Xu, H.; Zhang, H.; Kong, J.; Dresselhaus, M. S.; Zhang, J.; Liu, Z. *Nano Lett.* **2010**, *10*, 553−561.
(9) Ling, X.; Zhang, J. *Small* **2010**, *6*, 2020−2025.
(10) Xu, H.; Chen, Y. B.; Xu, W. G.; Zhang, H. L.; Kong, J.; Dresselhaus, M. S.; Zhang, J. *Small* **2011**, *7*, 2945−2952.
(11) Xu, H.; Xie, L. M.; Zhang, H. L.; Zhang, J. *ACS Nano* **2011**, *5*, 5338−5344.
(12) Yu, X.; Cai, H.; Zhang, W.; Li, X.; Pan, N.; Luo, Y.; Wang, X.; Hou, J. G. *ACS Nano* **2011**, *5*, 952−958.
(13) Huh, S.; Park, J.; Kim, Y. S.; Kim, K. S.; Hong, B. H.; Nam, J. M. *ACS Nano* **2011**, *5*, 9799−9806.
(14) Thrall, E. S.; Crowther, A. C.; Yu, Z.; Brus, L. E. *Nano Lett.* **2012**, *12*, 1571−1577.
(15) Qiu, C.; Zhou, H.; Yang, H.; Chen, M.; Guo, Y.; Sun, L. *J. Phys. Chem. C* **2011**, *115*, 10019−10025.
(16) Schlücker, S.; Kiefer, W. *Surface Enhanced Raman Spectroscopy: Analytical, Biophysical and Life Science Applications*; Wiley-VCH: New York, 2011.
(17) Schlücker, S. *ChemPhysChem* **2009**, *10*, 1344−1354.
(18) Wang, T.; Hu, X.; Dong, S. *Chem. Commun.* **2008**, 4625−4627.
(19) Li, J. F.; Huang, Y. F.; Ding, Y.; Yang, Z. L.; Li, S. B.; Zhou, X. S.; Fan, F. R.; Zhang, W.; Zhou, Z. Y.; Wu, D. Y. *Nature* **2010**, *464*, 392−395.
(20) Luo, J.; Cote, L. J.; Tung, V. C.; Tan, A. T. L.; Goins, P. E.; Wu, J.; Huang, J. *J. Am. Chem. Soc.* **2010**, *132*, 17667−17669.
(21) Hummers, W. S.; Offeman, R. E. *J. Am. Chem. Soc.* **1958**, *80*, 1339−1339.
(22) Zhang, Z.; Chen, H. H.; Xing, C. Y.; Guo, M. Y.; Xu, F. G.; Wang, X. D.; Gruber, H.; Zhang, B. L.; Tang, J. L. *Nano Res.* **2011**, *4*, 599−611.
(23) Marcano, D. C.; Kosynkin, D. V.; Berlin, J. M.; Sinitskii, A.; Sun, Z.; Slesarev, A.; Alemany, L. B.; Lu, W.; Tour, J. M. *ACS Nano* **2010**, *4*, 4806−4814.
(24) Li, D.; Muller, M. B.; Gilje, S.; Kaner, R. B.; Wallace, G. G. *Nat. Nanotechnol.* **2008**, *3*, 101−105.
(25) Sun, S.; Wu, P. *Phys. Chem. Chem. Phys.* **2011**, *13*, 21116−21120.
(26) Ghosh, A.; Rao, K. V.; Voggu, R.; George, S. J. *Chem. Phys. Lett.* **2010**, *488*, 198−201.
(27) Ramakrishna Matte, H.; Subrahmanyam, K.; Venkata Rao, K.; George, S. J.; Rao, C. N. R. *Chem. Phys. Lett.* **2011**, *506*, 260−264.
(28) Liu, Z. B.; Xu, Y. F.; Zhang, X. Y.; Zhang, X. L.; Chen, Y. S.; Tian, J. G. *J. Phys. Chem. B* **2009**, *113*, 9681−9686.
(29) Ghosh, A.; Rao, K. V.; George, S. J.; Rao, C. N. R. *Chem.—Eur. J.* **2010**, *16*, 2700−2704.
(30) Tang, Z.; Lei, Y.; Guo, B.; Zhang, L.; Jia, D. *Polymer* **2012**, *53*, 673−680.
(31) Yang, K.; Zhang, S.; Zhang, G.; Sun, X.; Lee, S.-T.; Liu, Z. *Nano Lett.* **2010**, *10*, 3318−3323.
(32) Qi, J.; Lv, W.; Zhang, G.; Zhang, F.; Fan, X. *Polym. Chem.* **2012**, *3*, 621−624.
(33) Middelhoek, E. R.; Zhang, H.; Verhoeven, J. W.; Glasbeek, M. *Chem. Phys.* **1996**, *211*, 489−497.
(34) Kovalenko, S. A.; Eilers-Konig, N.; Senyushkina, T. A.; Ernsting, N. P. *J. Phys. Chem. A* **2001**, *105*, 4834−4843.
(35) Ehrler, O. T.; Griffin, G. B.; Young, R. M.; Neumark, D. M. *J. Phys. Chem. B* **2009**, *113*, 4031−4037.
(36) Branigan, E. T.; Halberstadt, N.; Apkarian, V. *J. Chem. Phys.* **2011**, *134*, 174503.